

ORIGINAL ARTICLE

Pseudo-Computed Tomography Generation from Noisy Magnetic Resonance Imaging with Deep Learning Algorithm

Niloofer Yousefi Moteghaed^{1,2}, Ali Fatemi³, Ahmad Mostaar^{1,2*} 

¹ Department of Medical Physics and Biomedical Engineering, School of Medicine, Shahid Beheshti University of Medical Sciences, Tehran, Iran

² Radiation Biology Research Centre, Iran University of Medical Sciences, Tehran, Iran

³ Department of Physics, Jackson State University, Jackson, United States

*Corresponding Author: Ahmad Mostaar
Email: mostaar@sbmu.ac.ir

Received: 02 November 2022 / Accepted: 28 January 2023

Abstract

Purpose: Magnetic Resonance Imaging (MRI) applications offer superior soft tissue contrast compared with Computed Tomography (CT) for accurate radiotherapy planning although MRI images suffer from poor image quality and lack electron density for radiation dose calculation. The present study aims to use the Deep Learning (DL) approach to 1) enhance the quality of MRI images and 2) generate synthetic CT images using MRI images for more accurate radiotherapy planning.

Materials and Methods: In this paper, the pix2pix Generative Adversarial Network was utilized to synthesize CT images from noisy MRI images of 20 arbitrarily patients with brain disease. The standard statistical measurements investigated the accuracy comparison of the modeled Hounsfield Unit (HU) value from MRI images and referenced CT of each patient. The famous quality metrics that were used to compare synthetic CTs and referenced CTs were the Mean Absolute eError (MAE), the structural similarity index (SSIM), and the Peak Signal-to-Noise Ratio (PSNR).

Results: The higher quality measurements between the synthetic pseudo-CT and the referenced CT images as PSNR and SSIM should correlate with the lower MAE value. For the overall brain among blind test data, the measured peak signal-to-noise ratio, mean absolute error, and structural similarity index values were about 16.5, 28.13, and 93.46, respectively.

Conclusion: The proposed method provides an acceptable level of statistical measurements computed on the Pseudo-CT and referenced CT, and it could be concluded that the p-CT can be implemented in radiotherapy treatment planning with acceptable accuracy.

Keywords: Pseudo-Computed Tomography; Generative Adversarial Network; Deep Learning.

1. Introduction

Using Magnetic Resonance Imaging (MRI) is of growing interest in clinical oncology treatment planning routines. Despite the different advantages of the MRI modality in the MR-only radiotherapy approach, we face other challenges compared to traditional Computer Tomography (CT)-based radiotherapy approaches. In conventional radiotherapy workflow, anatomy acquisition, patient positioning, tumor and Organ At Risk (OAR) delineation, and dose calculation rely on CT images. But, the pixel value in MRI has no direct correlation with electron density, while the CT number can convert to electron density directly for the absorbed dose calculation procedure. However, before being used, medical images often need vital processes in pre-processing procedures, such as noise removal. As a result, noises and artifacts in MRI images can affect the whole process of MR-based treatment planning. Nowadays, a significant problem in image de-noising is distinguishing noise, edge, and texture since they all have high-frequency components. Recently, the improved hybrid approach [1-3] and deep neural networks have been used for the medical image de-noising methods [4, 5]. These networks do not need manually set parameters for removing the noise [6-16]. In recent years, various categories have been presented for MRI to CT conversions based on the sequences of MRI, region of imaging, and applications. In atlas-based ways, single [17] and multiple (containing several patients) [18-22] atlases are applied to estimate a Pseudo-CT) P-CT (without the requirement of a specific sequence of MRI. One of the main strengths of the atlas-based approach is that the patient's movement decreases due to the shorter scan time in a clinical setting. This approach focuses on aligning the MRI voxels and the value of the CT number or organ label. Next, there are model-based methods that include the use of standard or specific sequences such as ultra-short echo time imaging [23, 24] to investigate unusual anatomy, separation of bone from the air [25], and finding any relationship between the brightness intensity values of the MR and CT images [26, 27], or mapping from a given image to a specific target image with fuzzy logic approach [28, 29]. More recently, Deep Learning (DL) techniques have been developed for P-CT generation from MR images with high generalization ability and extrapolate results using standard MRI sequences.

Some researchers have trained image-to-image translation Convolutional Neural Networks (CNNs) [30-35], Generative Adversarial Networks (GAN) [36-41], Conditional GAN [42], and Cycle GAN [43-48], that try to learn the mapping from a given image to a specific target image for P-CT synthesis.

Accordingly, this study intends to generate P-CT images from noisy MRI images with deep learning algorithms. The MRI images contain random noises such as speckle noise and we are looking to better use MRI images for physicians and generate an appropriate P-CT image. Because an uncorrected MRI also creates uncorrected CT, and the error is transmitted throughout the process. The main goal of this study was to design a system that performs well when testing new data that may be contaminated with noise and obtains suitable P-CT data for MR-based radiotherapy.

2. Materials and Methods

We selected 20 brain tumor patients with routine T1W images from different centers without any effect on the treatment planning procedure. The MR images were prepared by a 1.5-Tesla scanner, with a range of 3.3-18 ms echo time, 280-550 ms repetition time, and slice thickness of 1.5-3 mm. On the other hand, the CT images of each person were prepared by a Siemens CT scanner using 120 kVp and a slice thickness of 1.5-3 mm with image matrix sizes of 512×512 for CT images. We tried to employ patients of different ages and genders with the age range of 29 years to 67 so that the trained model is not specific to a special group of people and we can have appropriate generalization ability during the test procedure. The number of female and male patients was the same in this study.

In the routine procedure, CT images of the patients are used as primary images in the treatment planning system, and MR images are used as auxiliary images for better delineation of tumors and organs at risk. In the radiotherapy treatment planning of brain tumors that almost tissues are soft and the differentiation between tumor and normal tissues is difficult, MRI is increasingly used owing to its superior soft-tissue contrast compared with CT. So it seems the use of MR-based treatment planning in brain tumors is more applicable and therefore in this study, P-CTs that contain CT information for treatment planning were generated from MRI images of the brain regions for each patient.

A pre-processing step plays an essential role in this type of study. The first stage of data preprocessing is MRI/CT data preparation. Furthermore, in the preprocessing section, the histogram-matched procedure and intensities normalization was used among all patients to standardize image intensities from different centers.

Also, a binary head mask was achieved from each MRI/CT image to mask a stereotactic head frame from CT images and the background region separation from MR images to have more accurate P-CT images. This would help us to decrease the overestimation error from predicted CT images. At last, all patient's images were registered to have peer-to-peer images. Training the deep learning model on aligned data is essential, as every MRI voxel should correlate with the same voxel in CT.

Before using MR to generate synthetic CT images, MR data must be corrected (de-noised) to find a suitable model for making updated P-CT images. We developed about 2500 2D slices of MRI images among 20 with synthetically added noise at 10-20% to generate "noisy" images. We randomly selected 2000 pairs of MRI images for the training/validation process and 500 images as synthetically unseen tests to evaluate the algorithm to find the best network. We proposed two series of DL algorithms to enhance MRI quality and generate P-CT images. This study presents the pix2pix-GAN (image-to-image translation GAN). It is an approach for training a deep convolutional neural network for image-to-image translation tasks that generally includes two subnetworks, a generator, and a discriminator field [49]. The Pix2Pix model is a conditional GAN type, where the output image's generation depends on the input. Our proposed structure consists of multiple convolution layers with batch normalization and activation functions to extract features of input images. The generator network learns a mapping to generate fake images, and the discriminator tries to discriminate whether the images are real or fake. We will use the best model saved at the end of the run, e.g., after ten epochs of training iterations. In Figure 1, we demonstrate our data flowchart process. The first network uses noisy MR images as input and references MRI images as output. The first DL network is trained to remove noise from MR images. On the other hand, the second DL network is trained based on the MR images as input and reference-CT scan images as output to create P-CT images.

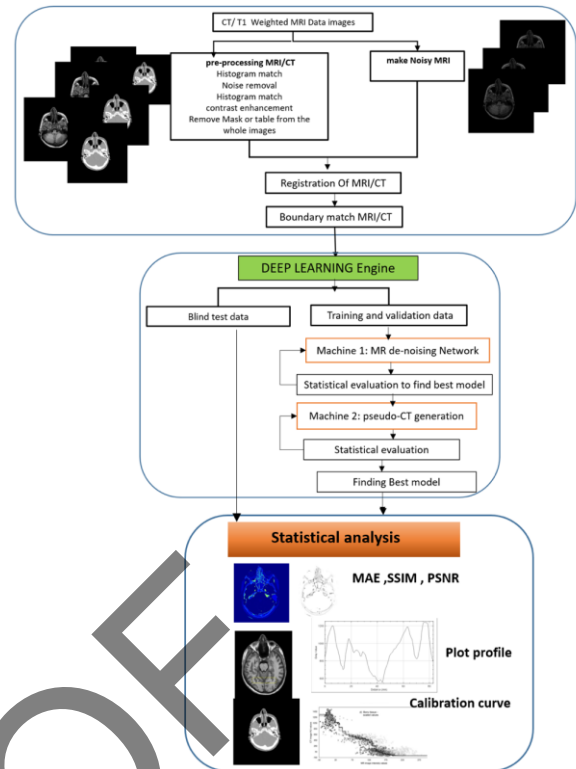


Figure 1. The flowchart of the proposed algorithm

Our proposed networks, trained with 2500 T1w images corrupted with noise, significantly improved the image quality based on different statistical analyses such as Peak Signal-to-Noise Ratio (PSNR), Structural Similarity Index Measure (SSIM), and Mean Absolute Error (MAE). The following statistical analysis is applied to the "**Corrected MR**" and "**P-CT**" images regarding mean and standard deviations of the MAE, SSIM, and PSNR computed on the entire head resulting from the pix2pixGAN methods.

The accuracy of the HU value of P-CT and true CT of each subject is evaluated by calculating the MAE of voxels in the brain region (Equation 1):

$$MAE(CT_{true}, P_CT) = \frac{1}{N} \sum_{i=1}^N |CT_{true}(i) - p_CT(i)| \quad (1)$$

Where N is the total number of voxels in the CT region, P_CT is the synthetic CT obtained by the deep learning method, and CT_{true} is a referenced image scanned by a CT scanner.

PSNR is most easily defined via the Mean Squared Error (MSE). For an actual CT image ($I (m \times n)$), its synthetic approximation (N), and the maximum possible pixel grayscale value of the CT images (MAX_I) the PSNR can be mathematically defined as (Equation 2):

$$PSNR = 10 \times \log_{10}\left(\frac{MAX_I^2}{MSE}\right) \quad (2)$$

$$MSE = \frac{1}{mn} \sum_{i=0}^{m-1} \sum_{j=0}^{n-1} [I(i,j) - N(i,j)]^2$$

In this paper, we have used SSIM to show the similarity of reference CT and P-CT with standard size $K \times K$ (Equation 3):

$$SSIM(CT, PCT) = \frac{(2\mu_{CT}\mu_{PCT} + c_1)(2\sigma_{CTPCT} + c_2)}{(\mu_{CT}^2 + \mu_{PCT}^2 + c_1)(\sigma_{CT}^2 + \sigma_{PCT}^2 + c_2)} \quad (3)$$

$$c_1 = (k_1L)^2, c_2 = (k_2L)^2, k_1 = 0.01, k_2 = 0.03$$

Where c_1 and c_2 are the constants to maintain stability, L is the dynamic range of the CT image grayscale, μ_x and μ_y are the mean of x , y , and σ_x^2 , σ_y^2 , and σ_{xy} are the variance and co-variance of x and y , respectively.

3. Results

The proposed framework has been tested on noisy MR images, and the performances were carried out using a five-fold cross-validation scheme and three major statistical measurements. Table 1 shows the statistics of quantitative comparison between noisy MR, corrected MR, true CT, and pseudo-CT images using five-fold cross-validation. The PSNR was compared between noisy MRI, modified MR, and P-CT images over the entire blind test data. Figures 2 and 3 show our DL algorithm results for T1w MR images with 10% to 20% noise artifacts. They offer the axial views of the generated enhanced MR images and the corresponding ideal and artifact-ridden MR images. The visual investigation revealed that the improved MR images generated by the model are less noisy and that P-CT has a higher similarity to the corresponding true CT images. While removing the artifact, our approach should preserve important microstructure details.

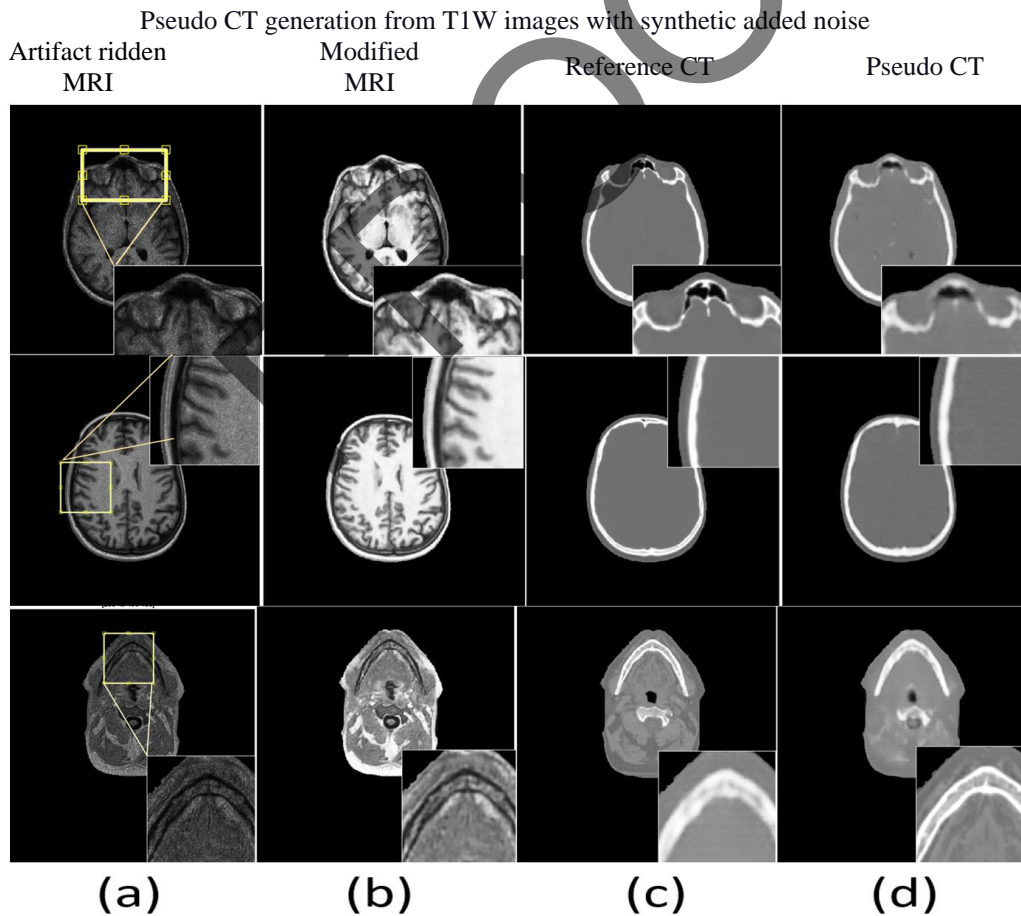
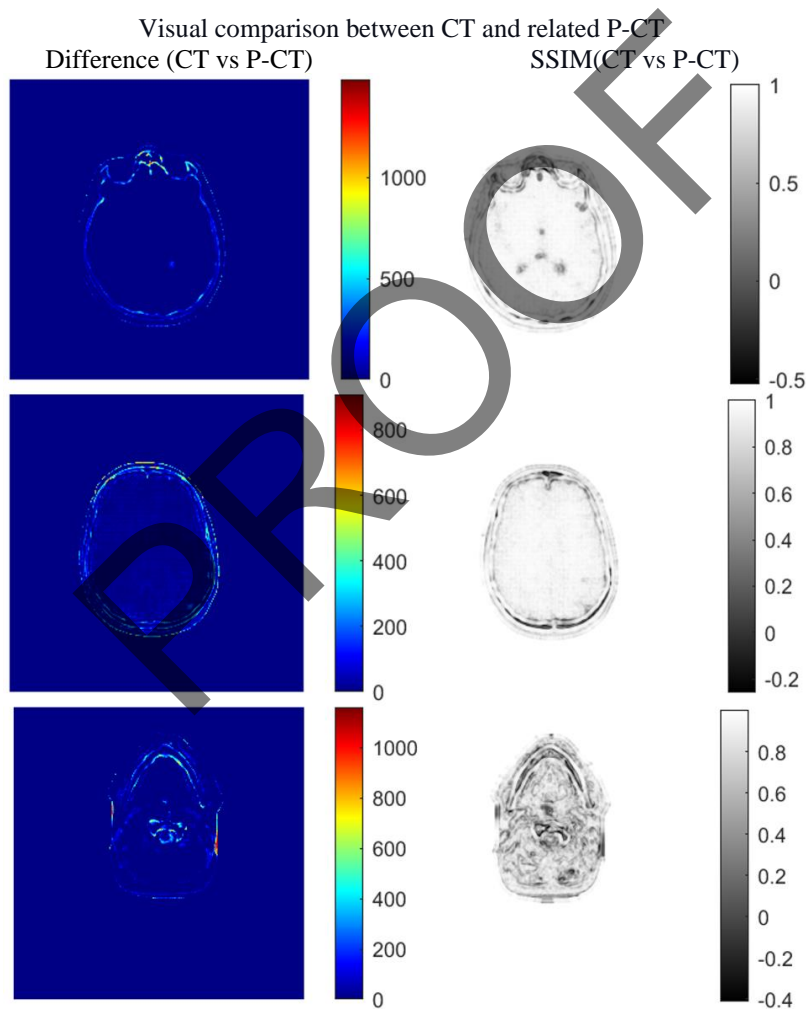


Figure 2. Qualitative comparison of enhanced and artifact-ridden images across different brain slices, for T1W MR images in axial view by proposed DL model: The figure indicates the full-frame images and the selected Region Of Interest (ROI) as shown on the bottom right in the yellow box of the corresponding images with the dimension of 512×512 . Images in different columns show (a) artifact-ridden MR images, (b) enhanced MR, (c) true CT, and (d) P-CT

Table 1. Statistics of quantitative comparison between ideal, modified, and artifact-ridden MRI images using five-fold cross-validation

Statistical Measurements (Average \pm Std) on Synthetic test data					
	MAE (\pm SD)	PSNR (Noisy MR) (\pm SD)	PSNR (Corrected MR) (\pm SD)	PSNR (P-CT) (\pm SD)	SSIM (P-CT) (\pm SD)
Fold 1	16.5 \pm 15.1	14.9 \pm 1.8	24.5 \pm 2.24	28.17 \pm 2.1	93.46 \pm 2.1
Fold 2	20.11 \pm 16.5	14.9 \pm 1.8	25.2 \pm 2.5	27.83 \pm 2.07	92.9 \pm 2.2
Fold 3	16.17 \pm 14.4	14.9 \pm 1.8	23.9 \pm 1.82	27.97 \pm 2.09	93.73 \pm 2.17
Fold 4	16.77 \pm 16.3	14.9 \pm 1.8	27.02 \pm 2.5	27.49 \pm 2.04	92.76 \pm 2.31
Fold 5	22.00 \pm 17.05	14.9 \pm 1.8	25.5 \pm 2.3	26.9 \pm 1.8	92.7 \pm 2.4

**Figure 3.** The difference and the SSIM map between P-CT and true CT image

In [Figures 4](#) and [5](#), we plot the line intensity profile and calibration curve over the same position for comparing experimental and simulated images as “true”, and “P-CT” images. The curve shows the relationship between the measured and Pseudo

Hounsfield unit. The best model for P-CT generation achieved better quantitative results of 16.5 \pm 15.1, 28.17 \pm 2.1, and 93.46 \pm 2.1 for MAE, PSNR, and SSIM, respectively.

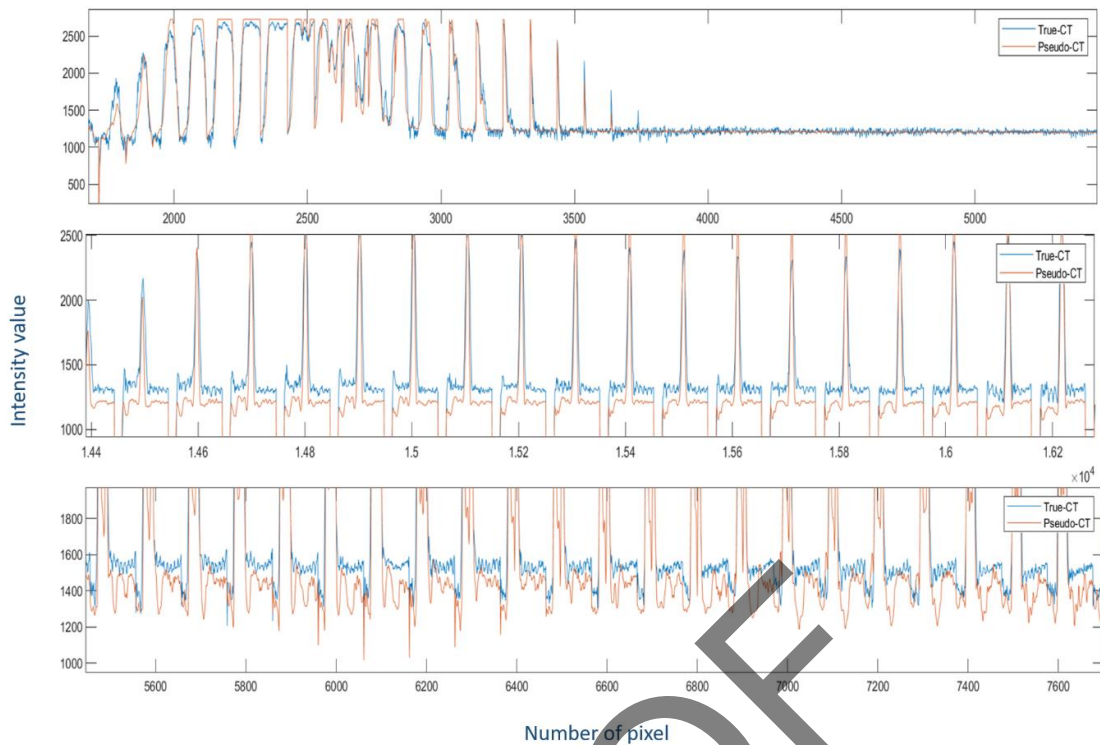


Figure 4. P-CT/ CT line profile on zoom region of the total selected profile

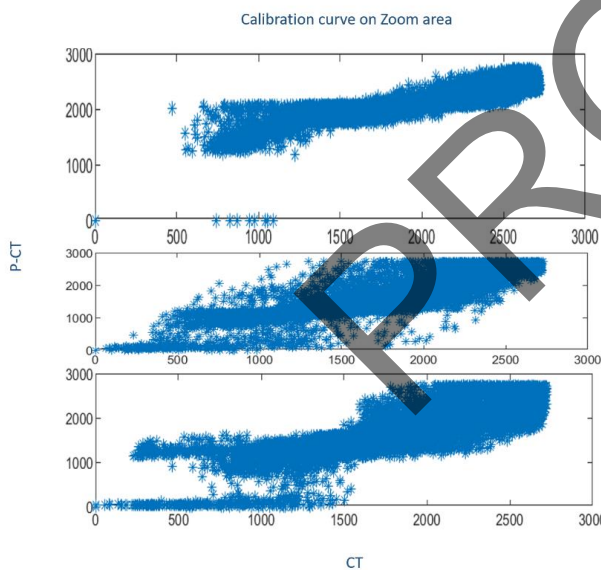


Figure 5. Calibration curve on the selected zoom area for P-CT/ CT

4. Discussion

The performance of proposed de-noising and simultaneous creation of P-CT algorithms are measured using quantitative or statistical measures as well as the visual quality of the images. There have been several published methods, each of which has its assumptions,

advantages, and limitations. An appropriate and ideal de-noising procedure requires a priori knowledge of the noise. In contrast, a practical system may not have sufficient information about the noise model or variance. This paper presents a noise level of 10%-20%. So better results for the MR image de-noising procedure are achievable by the proposed algorithm. The given hybrid deep learning model can generate a rapid synthesis of CT from a standard MRI sequence and high accuracy of Hounsfield unit value. The training and test data were randomly changed during the network training procedure to choose the best model. Still, all models were applied to the final blind test data to compare each model's performance better. According to the results, the amount of PSNR in noisy MR images is about 14; after applying each of the five implemented models, we reached 23-27. Also, on average, the PSNR value of P-CT images generated from noise-removed MR images is 28.17. The SSIM value of P-CT images compared to CT images is 93.46%, which indicates the proper performance of the algorithm.

Since MR images are obtained in different centers and may contain noise due to the scanning time or different slice thicknesses, this study aims to design an algorithm that simultaneously removes the noise from the test data and obtains P-CT images from MR images with reasonable accuracy. The results of the present study,

especially the SSIM analysis, provide a comprehensive comparison of the proposed algorithm and those from previously published sources. Therefore, we can easily apply the trained model to other test data from different centers to achieve better P-CT-generating performance. In the following, the main results of several studies have been compared with our proposed method based on the statistical measurements. For example, Yang *et al.* [43] propose a structure-constrained cycle-GAN and position-based selection strategy for selecting training images using unpaired data for brain MR-to-CT synthesis. They proposed methods that achieved to MAE value of 129. Tie *et al.* [40] achieved an MAE error of 75.7 using multi-channel multi-path conditional GAN to pseudo-CT generation from multi-parametric MR images.

The high the SSIM and PSNR, the lower the MAE values should be. In some of the articles, only the values of MAE are reported. In general, we have been

able to reach relatively good statistical results compared to other studies. For example, in Liang [47], the values of PSNR are better, but the image SSIM map value is lower compared to our article. Table 2 shows a more complete comparison of the results between the proposed method and some other studies as MAE, PSNR, and SSIM values.

5. Conclusion

A deep learning approach consisting of simultaneous training of conversion of noisy T1w MR images to de-noised MR and aligned P-CT images was employed. This work shows the feasibility of using P-CT images generated with a deep learning method based on pix2pix generative adversarial networks from noisy MR data. The image similarity between pseudo and true CT warrants further development of a MRI-only radiotherapy planning.

Table 2. Comparison of results between the proposed method and others such as MAE, PSNR, and SSIM values

Proposed works	Methods	MAE	PSNR	SSIM%
Yang <i>et al.</i> [1]	Structure-constrained cycle-GAN	129	24.15	77.7
Tie [2]	Multi-channel multi-path conditional GAN	75.7	-	-
Dinkla [3]	Dilated Convolutional Neural Network	75	-	-
Gupta [4]	3-Channel U-Net on Sagittal Images	81.02	-	-
Wang [5]	U-net deep learning algorithm with 23 convolutional layers	131	-	-
Wen Li [6]	CycleGAN network	74.5	27.3	73.3
Liang [7]	CycleGAN on CBCT	29.9	30.7	85
Zhang [8]	Generative Adversarial Network (GAN)	24	22	-
Li [9]	deep convolution neural network based on CBCT	6-27	-	-
Our proposed algorithm	Pix2pix GAN (image-to-image translation problems)	16	28.17	93.46

Acknowledgments

This project was supported by the Radiation Biology Research Center (RBRC) of the Iran University of Medical Sciences [Grant Number: 98-3-68-15603].

References

- 1- Jonas Lopes de Paiva, Claudio FM Toledo, and Helio Pedrini, "An approach based on hybrid genetic algorithm applied to image denoising problem." *Applied Soft Computing*, Vol. 46pp. 778-91, (2016).
- 2- N Yousefi Moteghaed, M Tabatabaeefar, A Mostaar, and Engineering, "Biomedical Image Denoising Based on

- Hybrid Optimization Algorithm and Sequential Filters." *Journal of Biomedical Physics*, Vol. 10 (No. 1), p. 83, (2020).
- 3- Deepa Bharathi and Sumithra Manimegalai Govindan, "A new hybrid approach for denoising medical images." in *Advances in Computing and Information Technology: Springer*, (2013), pp. 905-14.
 - 4- Pascal Vincent, Hugo Larochelle, Isabelle Lajoie, Yoshua Bengio, and Pierre-Antoine Manzagol, "Stacked denoising autoencoders: Learning useful representations in a deep network with a local denoising criterion." *Journal of machine learning research*, Vol. 11 (No. Dec), pp. 3371-408, (2010).
 - 5- Junyuan Xie, Linli Xu, and Enhong Chen, "Image denoising and inpainting with deep neural networks." in *Advances in neural information processing systems*, (2012), pp. 341-49.
 - 6- Kai Zhang, Wangmeng Zuo, and Lei Zhang, "FFDNet: Toward a fast and flexible solution for CNN-based image denoising." *IEEE Transactions on Image Processing*, Vol. 27 (No. 9), pp. 4608-22, (2018).
 - 7- Kai Zhang, Wangmeng Zuo, and Lei Zhang, "Learning a single convolutional super-resolution network for multiple degradations." in *Proceedings of the IEEE Conference on Computer Vision and Pattern Recognition*, (2018), pp. 3262-71.
 - 8- Heyi Li and Klaus Mueller, "Low-dose ct streak artifacts removal using deep residual neural network." in *Proceedings of Fully 3D conference*, (2017), Vol. 2017, pp. 191-94.
 - 9- Chunwei Tian, Lunke Fei, Wenxian Zheng, Yong Xu, Wangmeng Zuo, and Chia-Wen Lin, "Deep Learning on Image Denoising: An overview." *arXiv preprint arXiv:13171*, (2019).
 - 10- Chunwei Tian, Yong Xu, Lunke Fei, Junqian Wang, Jie Wen, and Nan Luo, "Enhanced CNN for image denoising." *CAAI Transactions on Intelligence Technology*, Vol. 4 (No. 1), pp. 17-23, (2019).
 - 11- Alice Lucas, Michael Iliadis, Rafael Molina, and Aggelos K Katsaggelos, "Using deep neural networks for inverse problems in imaging: beyond analytical methods." *IEEE Signal Processing Magazine*, Vol. 35 (No. 1), pp. 20-36, (2018).
 - 12- Fei L Tian C, Zheng W, Xu Y, Zuo W, Lin CW., "Deep learning on image denoising: An overview." *arXiv preprint arXiv:1912.13171*, (2019).
 - 13- Qingsong Yang *et al.*, "Low-dose CT image denoising using a generative adversarial network with Wasserstein distance and perceptual loss." *IEEE Transactions on Medical Imaging*, Vol. 37 (No. 6), pp. 1348-57, (2018).
 - 14- Venkata S Kadimesetty, Sreedevi Gutta, Sriram Ganapathy, Phaneendra K Yalavarthy, "Convolutional neural network-based robust denoising of low-dose computed tomography perfusion maps." *IEEE Transactions on Radiation and Plasma Medical Sciences*, Vol. 3 (No. 2), pp. 137-52, (2018).
 - 15- Ashkan Abbasi, Amirhassan Monadjemi, Leyuan Fang, Hossein Rabbani, Yi Zhang, "Three-dimensional optical coherence tomography image denoising through multi-input fully-convolutional networks." *Computers in biology and medicine*, Vol. 108pp. 1-8, (2019).
 - 16- Da Wang, Xuefeng Zhou, Zhihao Xu, Taobo Cheng, Xiaoxv Wang, and Haoqing Miao, "Ameliorated Deep Learning based on Improved Denoising Autoencoder and GACNN." in *2018 37th Chinese Control Conference (CCC)*, (2018): *IEEE*, pp. 9504-09.
 - 17- Benjamin Demol, Christine Boydev, Juha Korhonen, and Nick Reynaert, "Dosimetric characterization of MRI-only treatment planning for brain tumors in atlas-based pseudo-CT images generated from standard T1-weighted MR images." *Medical physics*, Vol. 43 (No. 12), pp. 6557-68, (2016).
 - 18- Johanna Degen and Mattias P Heinrich, "Multi-atlas based pseudo-ct synthesis using multimodal image registration and local atlas fusion strategies." in *Proceedings of the IEEE Conference on Computer Vision and Pattern Recognition Workshops*, (2016), pp. 160-68.
 - 19- Jens Sjölund, Daniel Forsberg, Mats Andersson, and Hans Knutsson, "Generating patient specific pseudo-CT of the head from MR using atlas-based regression." *Physics in Medicine & Biology*, Vol. 60 (No. 2), p. 825, (2015).
 - 20- Jason Dowling *et al.*, "Automatic MRI atlas-based external beam radiation therapy treatment planning for prostate cancer." in *International Workshop on Prostate Cancer Imaging*, (2010): *Springer*, pp. 25-33.
 - 21- Jinsoo Uh, Thomas E Merchant, Yimei Li, Xingyu Li, and Chiaho Hua, "MRI-based treatment planning with pseudo CT generated through atlas registration." *Medical physics*, Vol. 41 (No. 5), p. 051711, (2014).
 - 22- F Guerreiro *et al.*, "Evaluation of a multi-atlas CT synthesis approach for MRI-only radiotherapy treatment planning." *Physica Medica*, Vol. 35pp. 7-17, (2017).
 - 23- Eric D Morris *et al.*, "Using synthetic CT for partial brain radiation therapy: Impact on image guidance." *Practical radiation oncology*, Vol. 8 (No. 5), pp. 342-50, (2018).
 - 24- Yanle Hu *et al.*, "Magnetic resonance imaging-based treatment planning for prostate cancer: Use of population average tissue densities within the irradiated volume to improve plan accuracy." *Practical radiation oncology*, Vol. 5 (No. 4), pp. 248-56, (2015).
 - 25- Axel Largent *et al.*, "Comparison of deep learning-based and patch-based methods for pseudo-CT generation in MRI-based prostate dose planning." *International Journal of Radiation Oncology* Biology* Physics*, Vol. 105 (No. 5), pp. 1137-50, (2019).

- 26- Niloofar Yousefi Moteghaed, Ahmad Mostaar, Keivan Maghooli, Mohammad Houshyari, and Ahmad Ameri, "Estimation and evaluation of pseudo-CT images using linear regression models and texture feature extraction from MRI images in the brain region to design external radiotherapy planning." *Reports of Practical Oncology and Radiotherapy*, Vol. 25 (No. 5), pp. 738-45, (2020).
- 27- Niloofar Yousefi Moteghaed, Ali Yaghobi Joybari, and Ahmad Mostaar, "Pseudo-CT Generation for External Radiotherapy Planning from Magnetic Resonance Imaging Data on Brain Regions." *Iranian Journal of Radiology*, Vol. 16 (No. 3), (2019).
- 28- Niloofar Yousefi Moteghaed, Ahmad Mostaar, and Payam Azadeh, "Generating pseudo-computerized tomography (P-CT) scan images from magnetic resonance imaging (MRI) images using machine learning algorithms based on fuzzy theory for radiotherapy treatment planning." *Medical physics*, Vol. 48 (No. 11), pp. 7016-27, (2021).
- 29- A Largent et al., "A comparison of pseudo-CT generation methods for prostate MRI-based dose planning: deep learning, patch-based, atlas-based and bulk-density methods." *Physica Medica: European Journal of Medical Physics*, Vol. 68p. 28, (2019).
- 30- Maria Francesca Spadea et al., "Deep convolution neural network (DCNN) multiplane approach to synthetic CT generation from MR images—application in brain proton therapy." *International Journal of Radiation Oncology* Biology* Physics*, Vol. 105 (No. 3), pp. 495-503, (2019).
- 31- Anna M Dinkla et al., "MR-only brain radiation therapy: dosimetric evaluation of synthetic CTs generated by a dilated convolutional neural network." *International Journal of Radiation Oncology* Biology* Physics*, Vol. 102 (No. 4), pp. 801-12, (2018).
- 32- Shupeng Chen, An Qin, Dingyi Zhou, and Di Yan, "U-net-generated synthetic CT images for magnetic resonance imaging-only prostate intensity-modulated radiation therapy treatment planning." *Medical physics*, Vol. 45 (No. 12), pp. 5659-65, (2018).
- 33- Dinank Gupta, Michelle Kim, Karen A Vineberg, and James M Balter, "Generation of synthetic CT images from MRI for treatment planning and patient positioning using a 3-channel U-net trained on sagittal images." *Frontiers in oncology*, Vol. 9p. 964, (2019).
- 34- Yuenan Wang, Chenbin Liu, Xiao Zhang, and Weiwei Deng, "Synthetic CT generation based on T2 weighted MRI of nasopharyngeal carcinoma (NPC) using a deep convolutional neural network (DCNN)." *Frontiers in oncology*, Vol. 9p. 1333, (2019).
- 35- Yinghui Li et al., "A preliminary study of using a deep convolution neural network to generate synthesized CT images based on CBCT for adaptive radiotherapy of nasopharyngeal carcinoma." *Physics in Medicine & Biology*, Vol. 64 (No. 14), p. 145010, (2019).
- 36- Dong Nie et al., "Medical image synthesis with context-aware generative adversarial networks." in *International conference on medical image computing and computer-assisted intervention*, (2017): Springer, pp. 417-25.
- 37- Azin Shokraei Fard, David C Reutens, and Viktor Vegh, "CNNs and GANs in MRI-based cross-modality medical image estimation." *arXiv e-prints*, p. arXiv: 2106.02198, (2021).
- 38- V Bourbonne et al., "Dosimetric Validation of a GAN-Based Pseudo-CT Generation for MRI-Only Stereotactic Brain Radiotherapy. *Cancers* 2021, 13, 1082." ed: *s Note: MDPI stays neutral with regard to jurisdictional claims in published ...*, (2021).
- 39- Samaneh Kazemifar et al., "Dosimetric evaluation of synthetic CT generated with GANs for MRI-only proton therapy treatment planning of brain tumors." *Journal of applied clinical medical physics*, Vol. 21 (No. 5), pp. 76-86, (2020).
- 40- Xin Tie, Sai-Kit Lam, Yong Zhang, Kar-Ho Lee, Kwok-Hung Au, and Jing Cai, "Pseudo-CT generation from multi-parametric MRI using a novel multi-channel multi-path conditional generative adversarial network for nasopharyngeal carcinoma patients." *Medical physics*, Vol. 47 (No. 4), pp. 1750-62, (2020).
- 41- Yang Zhang et al., "Improving CBCT quality to CT level using deep learning with generative adversarial network." *Medical physics*, Vol. 48 (No. 6), pp. 2816-26, (2021).
- 42- Ke Xu et al., "Multichannel residual conditional GAN-leveraged abdominal pseudo-CT generation via dixon MR images." *IEEE Access*, Vol. 7pp. 163823-30, (2019).
- 43- Heran Yang et al., "Unpaired brain mr-to-ct synthesis using a structure-constrained cyclegan." in *Deep Learning in Medical Image Analysis and Multimodal Learning for Clinical Decision Support: Springer*, (2018), pp. 174-82.
- 44- Yang Lei et al., "MRI-only based synthetic CT generation using dense cycle consistent generative adversarial networks." *Medical physics*, Vol. 46 (No. 8), pp. 3565-81, (2019).
- 45- Yingzi Liu et al., "Liver synthetic CT generation based on a dense-CycleGAN for MRI-only treatment planning." in *Medical Imaging 2020: Image Processing*, (2020), Vol. 11313: *International Society for Optics and Photonics*, p. 113132L.
- 46- Hongfei Sun et al., "Imaging Study of Pseudo-CT Synthesized From Cone-Beam CT Based on 3D CycleGAN in Radiotherapy." *Frontiers in oncology*, Vol. 11p. 436, (2021).
- 47- Xiao Liang et al., "Generating synthesized computed tomography (CT) from cone-beam computed tomography (CBCT) using CycleGAN for adaptive radiation therapy."

Physics in Medicine & Biology, Vol. 64 (No. 12), p. 125002, (2019).

48- Wen Li *et al.*, "Synthesizing CT images from MR images with deep learning: model generalization for different datasets through transfer learning." *Biomedical Physics & Engineering Express*, Vol. 7 (No. 2), p. 025020, (2021).

49- Hazem Abdelmotaal, Ahmed A Abdou, Ahmed F Omar, Dalia Mohamed El-Sebaity, and Khaled Abdelazeem, "Pix2pix Conditional Generative Adversarial Networks for Scheimpflug Camera Color-Coded Corneal Tomography Image Generation." *Translational Vision Science & Technology*, Vol. 10 (No. 7), pp. 21-21, (2021).

PROOF